

# All-optical ultrafast switching of Si woodpile photonic band gap crystals

Tijmen G. Euser<sup>1,2</sup>, Adriaan J. Molenaar<sup>1,2</sup>, J. G. Fleming<sup>3</sup>,

Boris Gralak<sup>4</sup>, Albert Polman<sup>1</sup>, and Willem L. Vos<sup>1,2\*</sup>

<sup>1</sup>*FOM Institute for Atomic and Molecular Physics,*

*Kruislaan 407, 1098 SJ Amsterdam, The Netherlands*

<sup>2</sup> *Complex Photonic Systems, MESA<sup>+</sup> Research Institute,*

*University of Twente, The Netherlands*

<sup>3</sup> *Sandia National Laboratories, Albuquerque, NM, USA and*

<sup>4</sup> *Institut Fresnel, Marseille, France*

## Abstract

We present ultrafast all-optical switching measurements of Si woodpile photonic band gap crystals. The crystals are homogeneously excited, and probed by measuring reflectivity over an octave in frequency (including the telecom range) as a function of time. At short delay times  $< 200$  fs, we observe that the photonic gap becomes narrower than in the unswitched case. After 1 ps, the complete gap has shifted to higher frequencies. This intricate behavior is the result of competing refractive index changes due to an electronic Kerr nonlinearity and to optically excited free carriers. The frequency shift of the band gap as a function of pump intensity agrees well with exact modal method calculations. We briefly discuss possible applications.

PACS numbers: 42.70.Qs, 42.65.Pc, 42.79.-e

Currently, many efforts are devoted to a novel class of dielectric composites known as photonic crystals [1]. Spatially periodic variations of the refractive index commensurate with optical wavelengths cause the photon dispersion relations to organize in bands, analogous to electron bands in solids. Frequency windows known as stop gaps appear in which modes are forbidden for specific propagation directions. Fundamental interest in photonic crystals is spurred by the possibility of a photonic band gap, a frequency range for which no modes exist at all. Tailoring of the photonic density of states by a photonic crystal allows one to control fundamental atom-radiation interactions in solid-state environments [2, 3]. In this context the hallmark of a photonic band gap is the eagerly awaited full inhibition of spontaneous emission due to a vanishing density of states [2]. Additional interest is aroused by the possibility of Anderson localization of light by defects added to photonic band gap crystals [4].

Exciting prospects arise when photonic band gap crystals are switched on ultrafast timescales. In particular, switching photonic band gap crystals provides dynamic control over the density of states that would allow the switching-on or -off of light sources in the band gap [5]. Furthermore, switching would allow the capture or release of photons from photonic band gap cavities [5], which is relevant to solid-state slow-light schemes [6]. Switching the directional properties of photonic crystals also leads to fast changes in the reflectivity, where interesting changes have been reported for Bragg stacks [7, 8], 2D photonic crystals [9, 10], and first-order stop bands of 3D opaline crystals [11, 12]. Ultrafast control of the propagation of light is essential to applications in active photonic integrated circuits [13].

It is well-known that semiconductors have favorable properties for optical switching, hence they are excellent constituents for switchable photonic materials. Moreover, their elevated refractive indices are highly advantageous to photonic crystals *per se*. Therefore, we present in this Letter ultrafast all-optical switching experiments on Si woodpile photonic band gap crystals. The crystals are spatially homogeneously excited and probed by measuring reflectivity over broad frequency ranges (including the telecom range) as a function of time. At short delay times  $< 200$  fs, we observe that the photonic gap becomes narrower than in the unswitched case. After 1 ps, the complete gap has shifted to higher frequencies. This intricate behavior is the result of competing refractive index changes due to a third-order Kerr nonlinearity and to optically excited free carriers. Our experiments are compared to exact modal method calculations with experimentally constrained parameters [14].

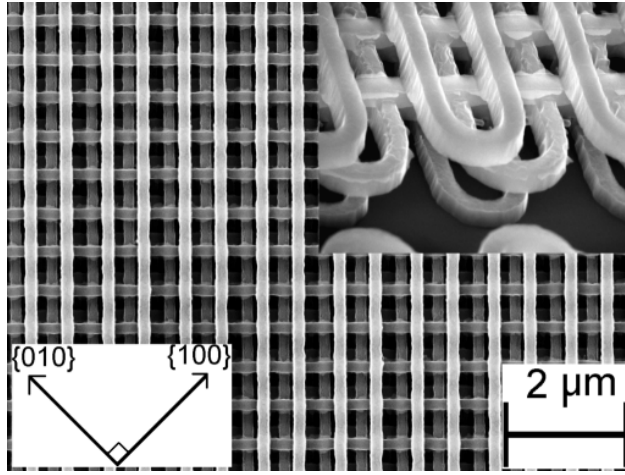


FIG. 1: High resolution scanning electron micrographs of a (001) surface of a Si woodpile crystal. The average lateral distance between two consecutive rods is  $650 \pm 10$  nm. The arrows indicate the crystal's (010) and (100) direction. Inset: side view of the crystal. The width and thickness of each rod is  $175 \pm 10$  nm and  $155 \pm 10$  nm respectively.

The Si woodpile photonic crystals are made using a layer-by-layer approach that allows convenient tuning of the operating wavelengths; here the crystals are designed to have a photonic band gap around the telecommunication wavelength of  $1.55 \mu\text{m}$  [15, 16]. High resolution scanning electron micrographs of a crystal are shown in Fig. 1. The crystals consist of five layers of stacked poly-crystalline Si nanorods that have a refractive index of 3.45 at  $1.55 \mu\text{m}$ . While each second rod in the crystal is slightly displaced by 50 nm, this periodic perturbation and the resulting superstructure do not affect the photonic band gap region [17]. Our measurements were reproduced on different crystals.

A successful optical switching experiment requires an as large as possible switching mag-

nitude, ultrafast time-scales, as low as possible induced absorption, as well as good spatial homogeneity [5]. In Si woodpile photonic crystals, optimum switching conditions are obtained for pump frequencies near the two-photon absorption edge of Si  $\omega/c = 5000 \text{ cm}^{-1}$  ( $\lambda = 2000 \text{ nm}$ ) [18]. Our setup consists of a regeneratively amplified Ti:Saph laser (Spectra Physics Hurricane) which drives two independently tunable optical parametric amplifiers (OPA, Topas). The OPAs have a continuously tunable output frequency between 3850 and 21050  $\text{cm}^{-1}$ , with pulse durations of 150 fs and a pulse energy  $E_{pulse}$  of at least 20  $\mu\text{J}$ . The probe beam is incident at normal incidence  $\theta = 0^\circ$ , and is focused to a Gaussian spot of 28  $\mu\text{m}$  FWHM at a small angular divergence  $\text{NA} = 0.02$ . The E-field of the probe beam is polarized along the (-110) direction of the crystal. The pump beam is incident at  $\theta = 15^\circ$ , and has a much larger Gaussian focus of 133  $\mu\text{m}$  FWHM than the probe, providing good lateral spatial homogeneity. We ensure that only the central flat part of the pump focus is probed. The reflectivity was calibrated by referencing to a gold mirror. A versatile measurement scheme was developed to subtract the pump background from the probe signal, and to compensate for possible pulse-to-pulse variations in the output of our laser [19].

Linear unpolarized reflectivity measurements of the crystal are presented as open squares in Fig. 2A. The broad stop band from 5600  $\text{cm}^{-1}$  to 8800  $\text{cm}^{-1}$  corresponds to the  $\Gamma$ -X stop gap in the band structure, which is part of the 3D photonic band gap of Si woodpile photonic crystals [14, 15]. The large relative width of  $\Delta\omega/\omega = 44\%$  shows that the crystals interact strongly with the light, in agreement with band gap behavior. While the crystals are relatively thin, the strong photonic interaction strength and the excellent crystal quality result in a high reflectivity of 95%, higher than in bulk Si and than in Si inverse opal photonic structures. The dashed curve in Fig. 2A represents an exact modal method calculation of the reflectivity in the (001) direction [14]. The measured Si rod dimensions, the displacements of individual layers, and the superstructure were included in our model. It is remarkable that the position and width of the stop band in our measurements and the theory agree well, since no parameters were freely adjusted.

Switched spectra were measured with our independently tunable OPAs as a function of probe delay  $\tau$  over an octave-broad probe frequency range  $\omega_{probe}$ . Our reflectivity measurements were reproduced on different positions on the crystal surface, and were compared to unswitched spectra. The resulting differential reflectivity of the crystal  $\Delta R/R(\tau, \omega_{probe})$  at ultrafast time scales is represented as a three-dimensional surface plot in Fig. 2B. At low fre-

quencies ( $6000\text{ cm}^{-1}$ ) and 1 ps after excitation, the reflectivity displays an ultrafast decrease  $\Delta R/R = -8\%$ , indicative of a shift of the stop band to higher frequencies. At intermediate frequencies near  $7000\text{ cm}^{-1}$ , the peak reflectivity of the stop band decreases by less than  $\Delta R/R = -1\%$ , confirming that the induced absorption is small, as opposed to experiments above the Si-gap where the absorption length  $>30\times$  shorter [11]. At high frequencies  $>8000\text{ cm}^{-1}$ , we observe intricate temporal behavior: near zero delay, a brief  $\approx 200\text{ fs}$  decrease in reflectivity ( $\Delta R/R = -5\%$ ) is followed by either a further decrease or by a strong increase up to  $\Delta R/R = 25\%$ , depending on frequency. The increase near  $9170\text{ cm}^{-1}$  (blue gap edge) confirms the shift of the whole gap. The 200 fs-decrease is attributed to an electronic Kerr nonlinearity, and was used to correct our temporal calibration for dispersion in the probe path. At probe frequencies near  $9400\text{ cm}^{-1}$ , strong variations in  $\Delta R/R$  with frequency are related to the shift of the superstructure feature (see Fig. 2A), that are also caused by large refractive index changes of the Si backbone. Compared to bulk Si at similar conditions, the photonic crystal structure results in  $10\times$  enhanced and dispersive reflectivity changes. Our observations lead to the striking conclusion that the photonic gap becomes narrow at ultrashort times, followed by a blue shift at slightly longer times.

To study the intricate ultrafast behavior in more detail, we have measured time traces at two characteristic frequencies, namely the red and blue edge of the stop band that are indicated by the red traces in Fig. 2B. The time delay curves of the calibrated absolute reflectivity changes  $\Delta R$  in Fig. 3 are measured over an extended time range. At the blue edge, a rapid decrease to  $\Delta R = -1\%$  appears within 190 fs, followed at 270 fs by an increase to  $\Delta R = 5\%$  within 500 fs. This increase is attributed to optically generated free carriers. The free carrier effect decays exponentially with a decay time of  $18 \pm 1\text{ ps}$ . The reflectivity at the red edge decreases by  $\Delta R = -12\%$  within 1 ps due to a Kerr nonlinearity, followed by a free carrier effect. At 2.5 ps after the excitation, the effect on the red edge decays exponentially to  $\Delta R = -1\%$  with a decay time of  $16 \pm 2\text{ ps}$ . The decay times of about 18 ps are much faster than carrier relaxation times in bulk Si, likely since our photonic crystals are made of poly-crystalline silicon, whose lattice defects and grain boundaries act as efficient carrier recombination traps [20].

It appears that the optical properties of excited Si are well described by the Drude model, which is valid for moderate electron densities in the range of our experiments [21]. In our model, the carrier density  $N_{eh} = 2 \times 10^{19}\text{ cm}^{-3}$ , and a Drude damping time  $\tau_{Drude}$  of 10 fs

were deduced by comparing the magnitude of the observed shift at 1 ps and the induced absorption in the stop band to exact modal method theory [14]. We infer a large maximum change in refractive index of the Si backbone  $\Delta n_{Si}/n_{Si}= 2\%$  at the red edge and  $\Delta n_{Si}/n_{Si}= 0.7\%$  at the blue edge. From our calculations we obtain the differential reflectivity of the photonic crystal versus probe frequency: the calculated changes at both stop band edges (Fig. 2C) agree well with the measured data in Fig. 2B. The good agreement between the calculated and measured switched spectra is connected to the notion from photonic bandstructure theory that the bandgap for our diamond-like photonic crystals appears in the frequency range of first-order stop gaps [15]. Conversely, for (inverse) opaline structures, the bandgap is predicted in the range of second-order stop gaps, where observed features are still awaiting a conclusive assignment [22]. This range is more sensitive to disorder [18], and no switching experiments have been reported in this range to date. Therefore, we conclude that woodpiles are suitable, switchable bandgap crystals.

To verify the nature of the switching mechanisms in the Si backbone of our crystals, we have studied the intensity scaling of the effects. Fig. 4B shows data from the initial Kerr nonlinearity at zero time delay. The linear scaling with pump intensity is consistent with a third-order Kerr nonlinearity. The Kerr coefficient  $n_2$ , is estimated by ratioing the reflectivity decrease at zero time delay (Fig. 3A) to the known free carrier effect at longer time delays  $\Delta n_{Si}/n_{Si} = -0.6\%$ , yielding  $n_2 = \frac{\Delta n_{Si}}{I_0} = \frac{3.5 \times 0.2\%}{16 \text{ GW cm}^{-2}} = 4.4 \pm 0.3 \times 10^{-13} \text{ cm}^2 \text{ W}^{-1}$ . To verify the free-carrier effects, the frequency shift of the blue edge of the stop band is plotted versus peak pump power squared  $I_0^2$  in Fig. 4A for a delay of 1 ps. We have also plotted data for the reflectivity feature at  $9750 \text{ cm}^{-1}$ . Both features shift linearly with the peak pump power squared, which confirms that a two-photon process is indeed the dominant excitation mechanism. From switched reflectivity spectra at 1 ps, we deduce a large maximum shift of the stop band edges of  $\Delta\omega_{red}/\omega_{red}= 2.4\%$  on the red edge at  $\omega_{red}= 5500 \text{ cm}^{-1}$ , while at  $\omega_{blue}= 9100 \text{ cm}^{-1}$  on the blue edge, the change  $\Delta\omega_{blue}/\omega_{blue}= 0.54\%$  is smaller, consistent with a Drude description of free carriers. From a comparison of the intensity scaling of the shift of the blue edge (Fig. 4A) to exact modal method theory, we obtain a two-photon absorption coefficient  $\beta= 60 \pm 15 \text{ cm GW}^{-1}$ . The corresponding large pump absorption length in the crystal exceeds 230 layers of rods, confirming that two-photon excitation of carriers yields much more homogeneously switched crystals than in one-photon experiments [11, 23].

In this paper, we demonstrate ultrafast switching and recovery of Si woodpile photonic band gap crystals at telecom wavelengths by all-optical electronic Kerr- and free carrier effects. Other interesting physical mechanisms have been proposed to change photonic crystals; including tuning by liquid crystals, which is inherently slow [24, 25], or heat-induced phase transitions, that seem to yield absorbing metallic states and slow recovery times [23]. In our switching experiments, we find unexpected non-monotonic physics: at short fs times, the photonic gap narrows, followed at longer ps times by a blue-shift of the gap. In other words, the blue edge of the gap shifts to lower frequency within the pulse duration, and subsequently shifts to higher frequency compared to the unswitched state, while the red edge only shifts to higher frequency. Consequently, the density of states near the blue edge of the band gap behaves more complex than predicted [5]. Consequently, we propose that a single pulse suffices to switch the DOS on by the Kerr effect, and rigorously off by free carriers on times governed by the pulse duration. Clearly, such versatile temporal density of states control will open exciting opportunities for timed QED lightsources whose emission is switched in absence of a cavity.

Since we have studied photonic crystals made with semiconductor fabrication techniques near the telecom frequency range, it is interesting to consider the applicability of on-chip ultrafast all-optical switching. Importantly, the pulse energy should be considerably reduced. This is feasible for devices such as modulators wherein a cavity resonance with quality factor  $Q$  is switched by one linewidth. Then, a small refractive index change  $\Delta n'/n' = 1/Q$  suffices. Assuming reported  $\lambda^3$ -sized cavities with  $Q = 10^4$  [26],  $\Delta n'/n'$  is 100 times smaller than in our experiments. By pumping with a diffraction limited pump pulse at above band gap frequencies ( $\omega_{pump} = 20000 \text{ cm}^{-1}$ ), free carriers are selectively excited inside the cavity volume only, requiring low pulse energies  $\leq 50 \text{ fJ}$ . Moreover, the observed decay times of less than 20 ps implies that switching could potentially be repeated at a rate  $\geq 25 \text{ GHz}$ . From heat diffusion theory, we estimate that the corresponding temperature increase in a Si sample is  $\leq 10 \text{ K}$  [27]. Therefore, we conclude that ultrafast photonic crystal switching also opens exciting opportunities in device applications.

We thank Cock Harteveld and Rob Kemper for technical support, Ad Legendijk and Dimitry Mazurenko for discussions, and Philip Harding for experimental help. This work is part of the research program of the "Stichting voor Fundamenteel Onderzoek der Materie" (FOM), which is supported by the "Nederlandse Organisatie voor Wetenschappelijk

Onderzoek” (NWO).

---

\* Electronic address: w.vos@amolf.nl; URL: [www.photonicbandgaps.com](http://www.photonicbandgaps.com)

- [1] 'Photonic Crystals and Light Localization in the 21<sup>st</sup> Century', Ed. C.M. Soukoulis (Kluwer, Dordrecht, 2001).
- [2] E. Yablonovitch, Phys. Rev. Lett. **58**, 2059 (1987).
- [3] P. Lodahl *et al.*, Nature **430**, 654 (2004).
- [4] S. John, Phys. Rev. Lett. **58**, 2486 (1987).
- [5] P.M. Johnson, A.F. Koenderink, and W.L. Vos, Phys. Rev. B **66**, 081102(R) (2002).
- [6] M.F. Yanik and S. Fan, Phys. Rev. Lett. **92**, 083901 (2004).
- [7] A. Haché and M. Bourgeois, Appl. Phys. Lett. **77**, 4089 (2000).
- [8] S.R. Hastings *et al.*, Appl. Phys. Lett. **86**, 031109 (2005).
- [9] S.W. Leonard, H.M. van Driel, J. Schilling, and R.B. Wehrspohn, Phys. Rev. B **66**, 161102(R) (2002); H.W. Tan, H.M. van Driel, S.L. Schweizer, R.B. Wehrspohn, and U. Gösele, *ibid.* **70**, 205110 (2004).
- [10] A.D. Bristow *et al.*, Appl. Phys. Lett. **83**, 851 (2003).
- [11] D. A. Mazurenko *et al.*, Phys. Rev. Lett. **91** 213903 (2003).
- [12] C. Becker *et al.*, Appl. Phys. Lett. **87**, 091111 (2005).
- [13] H. Nakamura *et al.*, Opt. Express **12**, 6606 (2004).
- [14] B. Gralak, M. de Dood, G. Tayeb, S. Enoch, and D. Maystre, Phys. Rev. E **67**, 066601 (2003).
- [15] K.M. Ho, C.T. Chan, C.M. Soukoulis, R. Biswas, and M. Sigalas, Solid State Commun. **89**, 413 (1994).
- [16] J.G. Fleming and S.Y. Lin, Opt. Lett. **24**, 49 (1999).
- [17] M.J.A. de Dood, B. Gralak, A. Polman, and J.G. Fleming, Phys. Rev. B **67**, 035322 (2003).
- [18] T.G. Euser and W.L. Vos, J. Appl. Phys. **97**, 043102 (2005).
- [19] The intensity of each pump and probe pulse is monitored by two photodiodes, and the reflectivity signal by a third photodiode. A boxcar averager holds the short output pulses of each detector for 1 ms, allowing simultaneous acquisition of separate pulse events of all three channels. Both pump and probe beam pass through a chopper that is synchronized to the repetition rate of the laser. The alignment of the two beams on the chopper blade is such that in



one sequence of four consecutive laser pulses, both pumped reflectivity, linear reflectivity, and two background measurements are collected. The pump-probe delay was set by a 40 cm long delay line with a resolution of 10 fs. At each frequency-delay setting, 4x250 pulse events were stored to increase the signal-to-noise ratio. From the resulting large data set, background was subtracted, and each reflected signal was referenced to its proper monitor signal to compensate for intensity variations in the laser output.

- [20] P.Y. Yu and M. Cardona, "Fundamentals of Semiconductors" (Springer Verlag, Berlin, 1996).
- [21] K. Sokolowski-Tinten and D. von der Linde, Phys. Rev. B **61**, 2643 (2000).
- [22] J.F. Galisteo-López and C. López, Phys. Rev. B **70**, 035108 (2004).
- [23] D.A. Mazurenko *et al.*, Appl. Phys. Lett. **86** 041114 (2005).
- [24] D. Kang *et al.*, Phys. Rev. Lett. **86**, 4052 (2001).
- [25] R. Sapienza *et al.*, Phys. Rev. Lett. **92**, 033903 (2004).
- [26] Y. Akahane, T. Asano, B-S Song, and S. Noda, Nature **425**, 944 (2003).

[27] **Calculated heating in high rep rate switching**

We consider an instantaneous point source of energy  $E_{pump} = 50$  fJ which is released in a photonic crystal cavity whose properties are assumed to be similar to bulk silicon. The temperature history of the cavity as a result of this single pump pulse at a distance  $r$  from the source is described by standard diffusion theory [28]:

$$\theta_{cav}(r, t) = \frac{E_{pump}}{8\rho c_p(\pi\alpha t)^{3/2}} \exp\left(-\frac{r^2}{4\alpha t}\right), \quad (1)$$

where  $\rho = 2330$  [kg/m<sup>3</sup>] the density,  $\alpha = 0.94$  [cm<sup>2</sup>/s] the diffusion constant, and  $c_p = 703$  [J/kgK] the heat capacity of silicon.

We now consider the situation in which a continuous series of pulses with energy  $E_{pump}$  is released into the cavity at a repetition rate of 25 GHz. The time between two pulses is  $\Delta t = 40$  ps. After  $N$  pulses, at time  $t = N\Delta t$ , the temperature distribution is given by:

$$\theta_{cav}(r, t) = \theta_0 + \theta_1 + \theta_2 + \dots + \theta_N. \quad (2)$$

To find the equilibrium temperature in the sample after many pulses, we evaluate Eq. 2 at a time  $t=(N+1)\Delta t$ , one cycle after the final pulse, and take the limit of the number of pulses going to infinity:

$$\theta(r, t) = \lim_{N \rightarrow \infty} \sum_{a=0}^N \frac{E_{pump}}{8\rho c_p (\pi\alpha((N+1)\Delta t - a\Delta t))^{3/2}} \exp\left(-\frac{r^2}{4\alpha((N+1)\Delta t - a\Delta t)}\right). \quad (3)$$

In the center of the cavity, at  $r=0$ , Eq. 3 reduces to:

$$\theta(r, t) = \lim_{N \rightarrow \infty} \sum_{a=0}^N \frac{E_{pump}}{8\rho c_p (\pi\alpha((N+1)\Delta t - a\Delta t))^{3/2}}. \quad (4)$$

Which can be simplified by bringing all constants pre factors out of the summation:

$$\theta(r, t) = \frac{E_{pump}}{8\rho c_p (\pi\alpha\Delta t)^{3/2}} \left( \lim_{N \rightarrow \infty} \sum_{a=0}^N \frac{1}{((N+1) - a)^{3/2}} \right), \quad (5)$$

The last factor of Eq. 5 is the well known Riemann Zeta function  $\zeta(s)$  [29]. In our case, where  $s= 3/2$ ,  $\zeta(s)$  evaluates to  $\zeta(3/2) \approx 2.612$ . The fixed prefactor (see Eq. 5) is equal to 2.972, yielding a temperature increase in the cavity of only  $2.972 \times 2.612 = 7.8$  K. We conclude that from the point of heat accumulation, the switching of a photonic crystal cavities with a continuous pulse train of weak 50 fJ pulses with an elevated repetition rate of 25 GHz seems perfectly feasible, and merits a study in its own.

[28] A. Bejan, Heat Transfer (John Wiley & Sons Inc., New York, 1993).

[29] M. Abramowitz and I. A. Stegun (Editors), Handbook of Mathematical Functions with Formulas, Graphs, and Mathematical Tables, (New York, Dover, pp. 807-808, 1972).

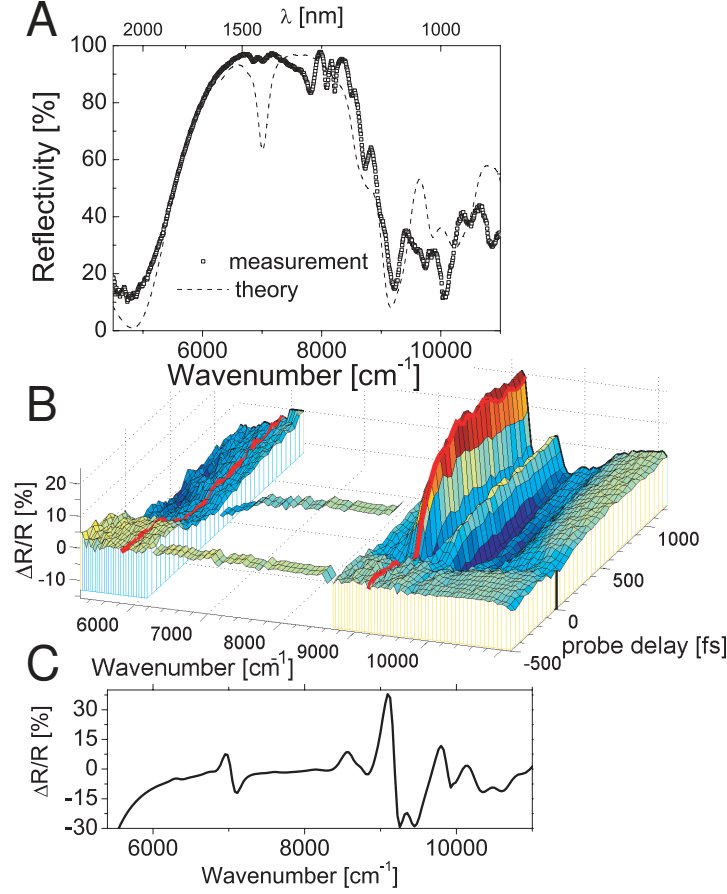


FIG. 2: (A) Linear unpolarized reflectivity measured in the (001) direction. A broad stop band with a maximum reflectivity of 95% appears for frequencies between  $5640 \text{ cm}^{-1}$  and  $8840 \text{ cm}^{-1}$ . The dashed curve represents an exact modal method calculation for polarized light, that agrees well with the linear measurements in the band gap region. (B) (color online) Differential reflectivity versus both probe frequency and probe delay. The pump peak intensity was  $I_0 = 17 \pm 1 \text{ GWcm}^{-2}$  on the red part,  $16 \pm 1 \text{ GWcm}^{-2}$  on the central part, and  $16 \pm 1 \text{ GWcm}^{-2}$  on the blue part of the spectrum. The probe delay was varied in steps of  $\Delta t = 50 \text{ fs}$ . The probe wavelength was tuned in  $\Delta\lambda = 10 \text{ nm}$  steps in the low, and central range, and in  $5 \text{ nm}$  steps in the high-frequency range. In the central part of the stop band,  $\Delta R/R(\omega)$  was measured at both negative delays and a positive delay of  $300 \text{ fs}$ . The red curves indicate fixed frequency curves along which extensive delay traces were measured. (C) Differential reflectivity changes versus probe frequency, calculated from exact modal method theory that includes the Drude model, and obtained by ratioing to the unswitched calculated spectrum shown in (A). The relative changes at the stop band edges agree quantitatively with the measured data in (B).

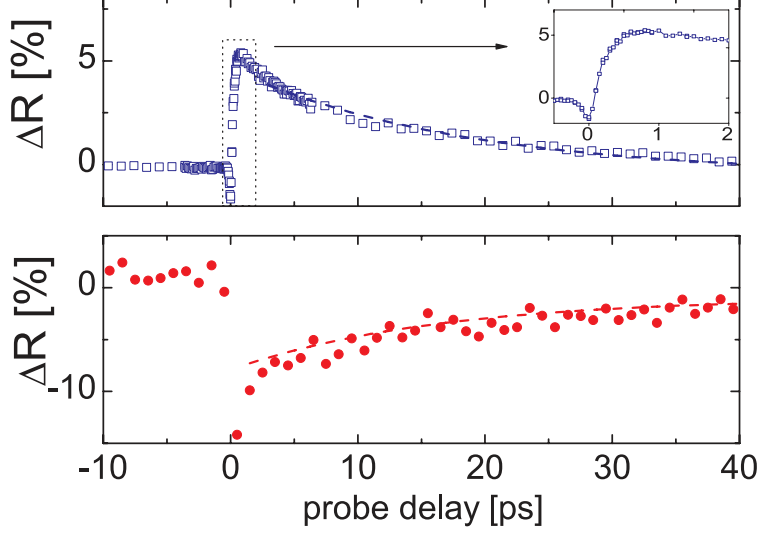


FIG. 3: (color online) Absolute reflectivity changes versus probe delay at frequency  $\omega_{blue} = 9174 \text{ cm}^{-1}$  at the blue edge of the gap (upper panel) and  $\omega_{red} = 5882 \text{ cm}^{-1}$  at the red edge (lower panel) of the gap. The pump intensity was  $I_0 = 16 \pm 1 \text{ GWcm}^{-2}$ . The dashed curves are exponential fits with a decay time of 18 ps (upper panel) and 16 ps (lower panel).

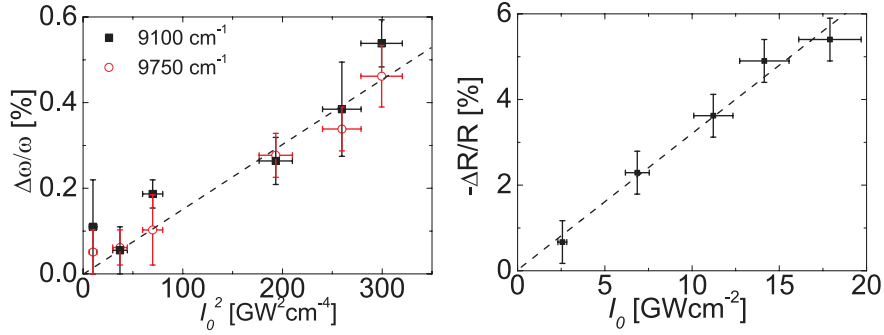


FIG. 4: (A) (color online) Squares: measured shift  $\Delta\omega/\omega$ , at  $\omega = 9100 \text{ cm}^{-1}$  on the blue edge of the stop band at 1 ps after excitation versus  $I_0^2$ . Diamonds:  $\Delta\omega/\omega$  measured at  $\omega = 9750 \text{ cm}^{-1}$ . The maximum observed shift is  $\Delta\omega/\omega = 0.54\%$ . The dashed curve serves to guide the eye. (B) Differential reflectivity decrease at  $\tau = 0$  on the blue edge of the stop band versus  $I_0$ . The reflectivity change scales linearly with  $I_0$ , consistent with a third-order Kerr nonlinearity. The dashed line is a least squares fit to the data.